ROYAL SOCIETY
OF CHEMISTRY

PAPER

Check for updates

A novel, recyclable magnetic biochar modified by chitosan–EDTA for the effective removal of Pb(II) from aqueous solution

Liwen Zheng, [ID] [ab] Yongchao Gao,*[b] Jianhua Du,[c] Wen Zhang,[b] Yujie Huang,[b] Leilei Wang,[b] Qingqing Zhao[b] and Xiangliang Pan*[a]

We report here the preparation process of a recyclable magnetic biochar functionalized with chitosan and ethylenediaminetetraacetic acid (E-CMBC). This prepared biochar was then evaluated regarding its adsorption performance for Pb(II) from an aqueous solution along with the potential adsorption mechanisms behind this process. XRD and SEM analyses showed that the magnetite particles were successfully embedded into biochar and the subsequent surface coating of chitosan and ethylenediaminetetraacetic acid modification were also successful. The effects of the adsorbent dosage, ionic strength, initial solution pH, and contact time, on adsorption kinetics, adsorption isotherms, adsorption thermodynamics and regeneration performance were investigated. The removal of Pb(II) was dramatically improved to 156.68 mg g^{-1} compared with that by unmodified pristine biochar (10.90 mg g^{-1}) at pH 3.0. In the range of pH 2.0–5.0, the adsorption performance of Pb(II) by E-CMBC remained above 152.50 mg g^{-1}, which suggested that the adsorption capacity of the novel sorbent was not impacted by the competing adsorption of hydrogen cations under acidic conditions. The adsorption process could be well described by the Avrami fractional-order and Langmuir models. Thermodynamic analysis proved that the adsorption process was spontaneous and endothermic. The magnetic strength of E-CMBC was measured as 3.1 emu g^{-1}, suggesting that the consumed E-CMBC could be separated from water by an external magnet. A regeneration study showed that after three cycles of adsorption–desorption, 78.60% of the sorbent was recovered and 97.26% of the adsorption capacity was retained. The adsorption mechanism investigation indicated that Pb(II) adsorption was mainly due to the presence of functional amides and carboxyl groups of E-CMBC forming strong chemical complexation. In conclusion, E-CMBC is a novel, recyclable, and highly efficient adsorbent for removal of Pb(II) from aqueous solution.

1. Introduction

Lead is one of the most widespread heavy metals polluting the environment and enters surface and ground water through a variety of ways, including emissions from burning fossil fuels, fertilizer application, wastewater discharge (*e.g.*, originating from mining, smelting, and chemical and battery manufacturing industries), and waste dumping and disposal.[1–6] It is of particular concern due to its great toxicity, non-biodegradability and tendency to accumulate in living organisms.[7–13] Once present in a living system, lead poisoning damages basic cellular processes and affects tissue and organ systems including the kidney, brain, liver and other organs.[14–17] Given this severity, Pb(II) removal form wastewater is necessary before it is discharged into the environment.

Numerous treatment technologies have been successfully applied for the removal Pb(II) from aqueous solutions, such as chemical precipitation,[18] ion exchange,[17,19] electrochemical treatment,[20] membrane filtration,[21] and adsorption.[17,22] Of these, adsorption is considered one of best methods for Pb(II) removal from aqueous solutions owing to its ease of use and high efficiency.[23] Various absorbents have been used for Pb(II) removal from aqueous solutions, such as activated carbon,[24] carbon nanotubes,[25] graphene,[26] and cation-exchange resins.[27] However, these adsorbents have several disadvantages, including high production costs, low adsorption efficiency for Pb(II) and difficulty in recycling and reuse. Collectively, these limit the application of these adsorbents. As a result, recent years have seen extensive work to develop cheap and widely available adsorbents.[28]

[a]College of Environment, Zhejiang University of Technology, Hangzhou 310032, PR China. E-mail: xiangliangpan@163.com

[b]Qilu University of Technology (Shandong Academy of Sciences), Ecology Institute, Shandong Provincial Key Laboratory of Applied Microbiology, Jinan 250103, PR China. E-mail: gaoyc@sdas.org

[c]Global Centre for Environmental Remediation, Faculty of Science, University of Newcastle, Callaghan, NSW 2308, Australia

Biochar is the carbonaceous product of the pyrolysis of organic matter and has received significant attention recently, owing to its low cost, abundance of raw materials, and convenient preparation. However, like other conventional adsorbents, the recycling difficulty of powdered biochar had restrained its wider application.[29] Although past work attempted to introduce magnetic properties to biochar,[30,31] these efforts greatly impacted the adsorption ability of the resulting magnetic biochar. For instance, Son *et al.* developed an engineered magnetic biochar by impregnating waste marine macroalgae with iron oxide particles (*e.g.*, magnetite, maghemite). The resulting biochar had removal efficiency for heavy metals that decreased from 70 mg g^{-1} to 56 mg g^{-1}.[32]

Chitosan is an abundant, biodegradable, non-toxic, and natural product derived from shells of shrimp and other sea crustaceans.[33] It has been intensively studied for the removal of heavy metals from aqueous solutions since its amine functional groups have strong bonding abilities.[34] However, the poor solubility, low stability and separability from aqueous solutions after adsorbing heavy metals limited the application of chitosan.

Despite these past limitations, using chitosan to modify the surface of magnetic biochar would combine the advantages of magnetic biochar with the positive attributes of chitosan, namely, its porous network, easy separability, and high chemical affinity. To this end, Xiao *et al.* prepared a chitosan-combined magnetic biochar. The resulting biochar showed high Cr(VI) and Cu(II) adsorption capacities of 30.14 mg g^{-1}, and 54.68 mg g^{-1}, respectively.[35] To further increase the adsorption capacity, of chitosan, past work has also focused on chemically modifying chitosan adsorbents,[36] however, there are few studies that have focused on the chemical modification of chitosan-combined magnetic biochar.

Ethylenediaminetetraacetic acid (EDTA) is a widely used complexing agent. Importantly, it effectively removes heavy metals through its metal complexing mechanism. Various materials modified with EDTA have had greatly improved adsorption capacities for heavy metals.[37] However, there are no studies investigating Pb(II) adsorption by EDTA-modified, chitosan-combined magnetic biochar.

In this study, we functionalized a novel, chitosan-combined magnetic biochar adsorbent through chemical modification with EDTA. This was done to achieve Pb(II) removal from an aqueous solution. After the carboxyl groups of EDTA reacted with the amino groups on chitosan, a large amount of acid amides and carboxyl groups were added to the surface of the chitosan-combined magnetic biochar. Critically, this may improve the affinity of chitosan to aqueous Pb(II).[34] Given this, the objectives of this work were as follows: (1) preparation and characterization of the modified biochar, (2) investigation of the Pb(II) removal performance of the modified biochar, (3) analysis of the Pb(II) adsorption mechanism of the modified biochar, and (4) assessment of the regeneration and reusability of the modified biochar.

2.   Materials and methods

2.1   Materials

For the feedstock biomass of the biochar, peanut shells were obtained from Taian, Shandong Province, China. All chemicals and reagents utilized in these experiments were of analytical grade. Ferric chloride hexahydrate (FeCl$_3$·6H$_2$O) and acetic acid were purchased from SonoPharm Chemical Reagent Co. Ltd. (Shanghai, China). 1-Ethyl-3-(3-dimethylaminopropyl) carbodiimide hydrochloride (EDAC), ethylenediaminetetraacetic acid disodium salt (Na$_2$EDTA), chitosan, EDTA, and Pb(NO$_3$)$_2$ were all purchased from Aladdin Reagent Co. Ltd. (Shanghai, China). An aqueous stock solution of 1000 mg L^{-1} Pb(II) was prepared by dissolving specific amounts of Pb(NO$_3$)$_2$ in deionized water.

2.2   Preparation of modified biochar

The modified biochar was synthesized using a step-by-step approach as shown in Fig. 1. The method to synthesize this magnetic biochar was based on previous work by Zhang *et al.*[38]
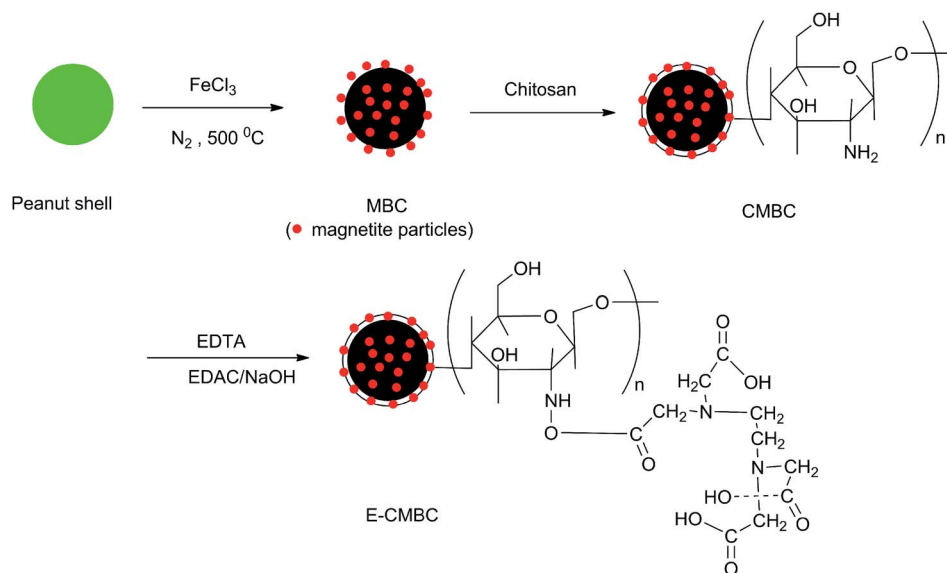

Fig. 1   Schematic for the preparation of MBC, CMBC, and E-CMBC.

Briefly, the peanut shell was air-dried, milled, and sieved (<1 mm). The treated peanut shell was then divided into two parts. One part remained untreated and the other part was added to 500 mL of 1 mol L^{-1} FeCl$_3$ solution and stirred for 24 h at room temperature. The filter residue was oven-dried at 70 °C for 2 h. Both the FeCl$_3$ treated and non-treated pristine peanut shells were pyrolyzed in a furnace at 500 °C for 2 h in N$_2$ atmosphere with a heating rate of 5 °C min^{-1}. The products of the non-treated and pre-treated peanut shells are referred to as BC and MBC, respectively.

The chitosan-modified magnetic biochar (CMBC) was prepared by the using a coating process described previously with minor alterations to allow its optimization for this study.[29] Briefly, 3.0 g chitosan was dissolved in 300 mL of 2% (v/v) acetic acid solution. Then, 3.0 g prepared MBC was added into the solution, after which the mixture was stirred for 2 h. Drop-wise condensation of 1% NaOH was added to the homogenous mixture until the pH reached 10. The mixture was then maintained at room temperature overnight, after which it was washed with deionized water to remove any excess NaOH. Lastly, the chitosan-modified magnetic biochar was separated and oven-dried at 70 °C.

Next, 1.0 g of CMBC and 1.0 g of EDTA were added into 100 mL of deionized water and then stirred at 60 °C for 4 h, then the mixed solution was cooled down to 40 °C. Afterwards, 5 mL of 1 mol L^{-1} NaOH and 0.96 g EDAC were added in an orderly manner. The solution was stirred at 40 °C for 2 h, and then stirred at room temperature overnight. After stirring, the solution was filtered and the materials were successively washed with 0.1 mol L^{-1} NaOH, deionized water, 0.1 mol L^{-1} HCl, and then deionized water to be neutral. After this series of washes, the materials were oven-dried at 70 °C. Samples were sieved through a 100-mesh screen and sealed to preserve them prior to use. This resulting chitosan and EDTA modified magnetic biochar is referred to as E-CMBC.

2.3 Characterization of the biochars

The surface morphologies of the samples were characterized by scanning electron microscopy (SEM) (Carl Zeiss AG., Germany). The Brunauer–Emmett–Teller (BET) surface area and the total pore volume were measured from N$_2$ isotherms using a surface area and porosimetry analyzer (Quantachrome Instruments, USA). Surface chemical composition of the samples was confirmed by X-ray photoelectron spectroscopy (XPS) (Thermo Fisher Scientific, USA). The Fourier transform infrared spectroscopy (FTIR) of the samples was measured on a spectrophotometer (Thermo Fisher Scientific, USA) using KBr pellets in the range of 400–4000 cm^{-1}. The X-ray diffraction (XRD) patterns of the samples were examined by an X-ray diffractometer with Cu Kα radiation (Rigaku Corporation, Japan). The zeta potential was measured at a range of 1–5 using a zeta potential analyzer (Malvern Instruments Ltd., United Kingdom). The magnetization measurement of E-CMBC was performed using a vibrating sample magnetometer (VSM) (Lake Shore Cryotronics, Inc. USA).

2.4 Adsorption experiments

All batch experiments were conducted in a 50 mL conical flask by mixing 1 g L^{-1} biochar with 25 mL Pb(II) aqueous solution on a rotary shaker at 150 rpm. The pH of the initial solutions was adjusted using either HCl or NaOH, as appropriate. The concentration of residual Pb(II) was determined using an Agilent 240FS AA atomic absorption spectrometer.

The dosage effect of E-CMBC was tested in the range of 0.2–2.0 g L^{-1} for Pb(II) removal at pH 3.0 and 298 K for 24 h. Both BC and E-CMBC were used to study the effect of pH on Pb(II) adsorption. The effect of pH was studied by adjusting the pH of the initial Pb(II) solution (200 mg L^{-1}) to values in the range of pH 1.0–5.0. The pH was adjusted to the desired value by adding negligible volumes of either HCl or NaOH, as appropriate. Flasks were then shaken at 298 K for 24 h. The effect of ionic strength was studied at pH 3.0 and 298 K for 24 h, with Pb(II) concentration of 200 mg L^{-1}. Kinetic experiments were performed at different time intervals, ranging from 10 to 2880 min, with 200 mg L^{-1} Pb(II) solutions at pH 3.0. Adsorption isotherms were determined within a set concentration range (20–500 mg L^{-1}) for 24 h at pH 3.0. These studies were conducted at 298 K, 308 K, and 318 K.

The adsorption amount q_e (mg g^{-1}) of Pb(II) was calculated using the following equation:

$$q_e = \frac{c_0 - c_e}{m} \times V \tag{1}$$

where c_0 (mg L^{-1}) is the initial concentration, c_e (mg L^{-1}) is the concentration at equilibrium, V (L) is the volume of the solution, and m (g) is the amount of the adsorbent.

All the experiments were conducted in triplicate under identical conditions and the average values are presented here. The relative errors of the dada were within 5%.

2.5 Regeneration studies

To evaluate their reusability, E-CMBC samples were tested by successive Pb(II) adsorption and desorption cycles. After attaining equilibrium, Pb(II) laden E-CMBC was separated from the solution and eluted using deionized water, then stirred in 0.1 mol L^{-1} Na$_2$EDTA solution overnight. The E-CMBC was filtered and thoroughly washed with deionized water, after which it was oven-dried. The regenerated E-CMBC was then successively subjected to two times of adsorption–desorption cycles.

3. Results and discussion

3.1 Characterization of the biochars

Biochar surface properties are important for its inherent reactivity and the surface morphologies of BC, MBC, CMBC, and E-CMBC from this study are shown in Fig. 2. BC had a smooth, layered, and porous structure. After being disposed by FeCl$_3$, the surface of MBC formed smaller pore channels. Metal clusters were clearly observed on both surface and within the pore channel of MBC. This indicated that the magnetic particle had been assembled on the surface of MBC. The surface of CMBC became thicker, appearing as if the surface was covered, and the pore channel was blocked. After the EDTA modification, there were increased numbers of different particles on the E-CMBC surface and its irregular surface became much rougher in appearance.
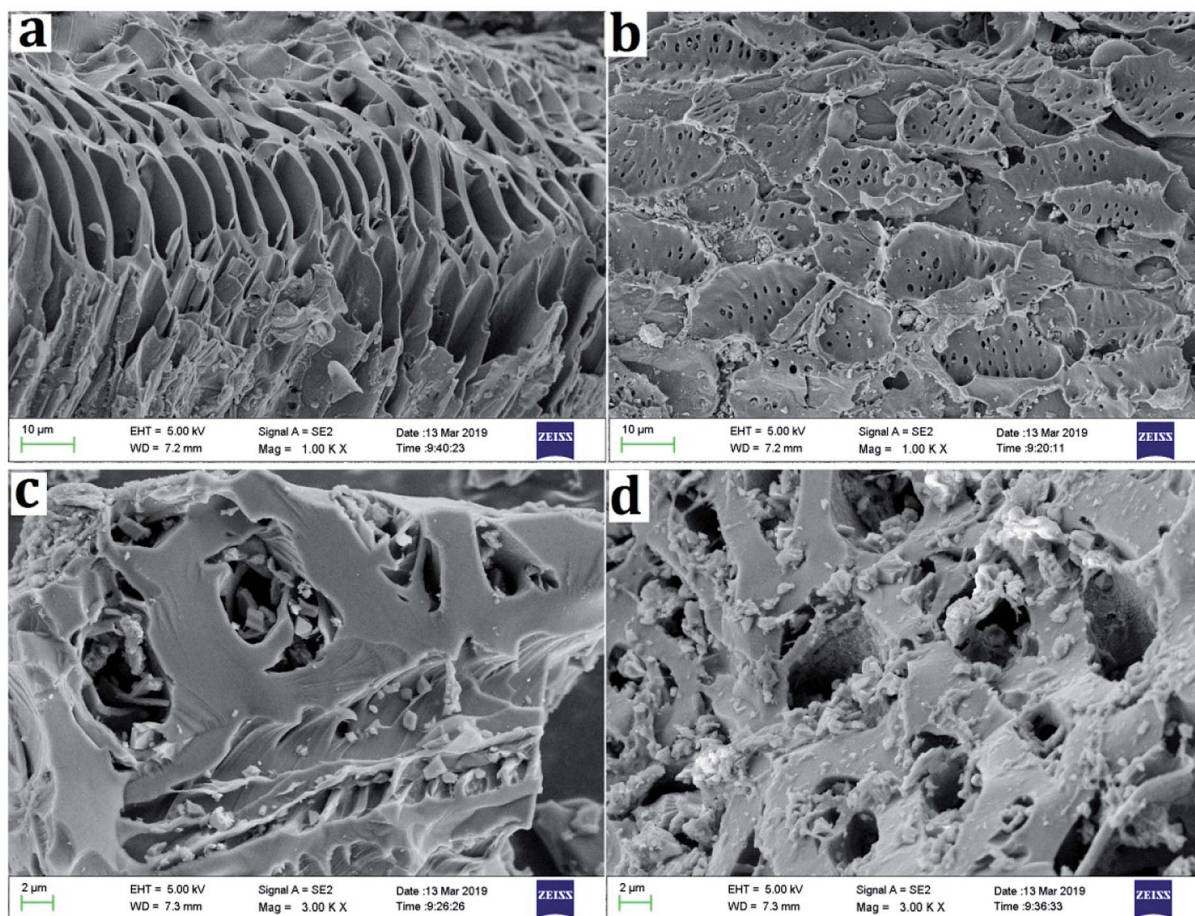
Fig. 2 Representative SEM images of (a) BC, (b) MBC, (c) CMBC, and (d) E-CMBC.

Table 1 presents the surface area, pore volume and average pore size of BC, MBC, CMBC and E-CMBC. The surface area of BC was larger ($231.38 \ m^2 \ g^{-1}$) than that of MBC ($11.63 \ m^2 \ g^{-1}$), CMBC ($1.64 \ m^2 \ g^{-1}$), or E-CMBC ($3.09 \ m^2 \ g^{-1}$). These results indicated that the modification yielded a dramatic decrease in specific surface area. Similar results were apparent in different pore volumes (Table 1). Contrastingly, the average pore sizes of MBC, CMBC, and E-CMBC were all larger than that of BC. This is likely due to the blockage of some of the smaller pores of the biochar by the magnetic particles and chitosan.[39]

The chemical compositions of BC and E-CMBC were determined by XPS and the XPS full spectra are shown in Fig. 3a. For BC, the three peaks at approximately 291.68 eV, 406.28 eV, and 537.48 eV corresponded to C 1s (81.35%), N 1s (1.43%) and O 1s (17.22%), respectively. After modification, a new peak at approximately 736.78 eV was Fe $2p_3$ (0.6%), which indicated the successful blending of the biochar with iron oxide in E-CMBC. The E-CMBC sample also had higher contents of N 1s (6.31%) and O 1s (25.1%) when compared with BC, which indicated that the EDTA was successfully introduced into the surface of the CMBC.

The FTIR spectra verified the existence of abundant functional groups in E-CMBC. As shown in Fig. 3b, the broadband of approximately 3416 cm^{-1} was assigned to the stretching vibrations of –OH groups along with the overlapping stretching vibrations of the –NH$_2$ groups. The band at 2911 cm^{-1} was assigned to the stretching vibrations of the aliphatic –CH– group.[34] The band at

Table 1 Pore distribution properties and Pb(II) adsorption capacities of BC, MBC, CMBC, and E-CMBC

Biochar	BET surface area ($m^2 \ g^{-1}$)	Pore volume ($cm^3 \ g^{-1}$)	Average pore size (nm)	Pb(II) adsorption capacity[a] ($mg \ g^{-1}$)
BC	231.38	0.05	2.46	17.10
MBC	11.63	0.029	10.98	22.05
CMBC	1.64	0.012	29.26	39.50
E-CMBC	3.09	0.015	20.57	156.80

[a] Experimentally measured value at a shaking speed of 150 rpm and 298 K for 24 h and at the original solution pH.
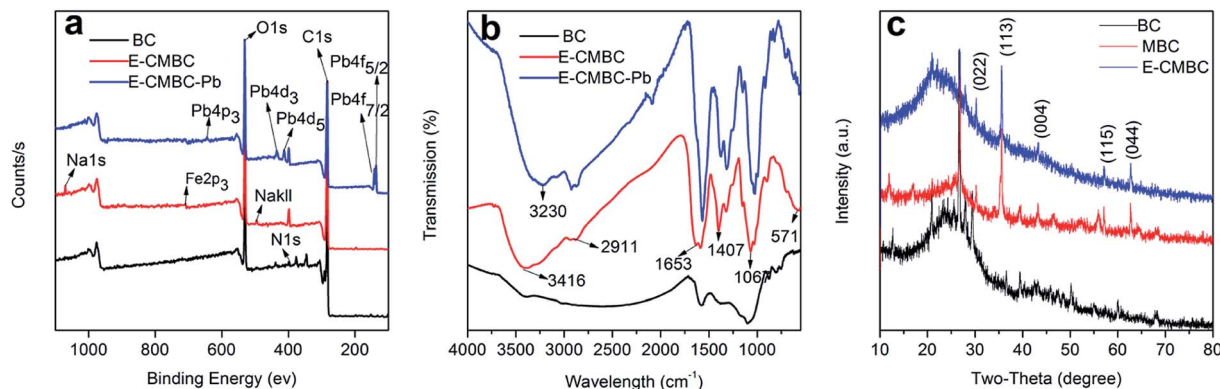
Fig. 3 (a) XPS survey spectra of BC, E-CMBC, and loading Pb(ii) (E-CMBC-Pb); (b) FTIR spectra of BC, E-CMBC, and loading Pb(ii) (E-CMBC-Pb); (c) XRD patterns of BC, MBC, and E-CMBC.

1635 cm^{-1} corresponded to the C=O stretching vibration of either –NH–C=O or –COOH. The characteristic band appeared at 1407 cm^{-1} was the C–O stretching vibrations of the –COOH group.[40] The band at 1067 cm^{-1} was related to the stretching vibration of both C–O and C–C.[34] Taken together, the aforementioned peak bands indicated that the biochar surface coating of chitosan and subsequent EDTA modification to its surface were both successful. Furthermore, the band at 571 cm^{-1} was assigned to the Fe–O stretching vibration,[39] which indicated that the magnetization process of the biochar was successful. Notably, the functional groups of E-CMBC were different from those of BC, which impacted its subsequent adsorption ability.

XRD spectra are shown in Fig. 3c. There were five intense characteristic peaks for MBC at $2\theta = 30.1°$, $35.4°$, $43.1°$, $56.9°$, and $62.5°$, which corresponded to the primary diffraction of the (022), (113), (004), (115) and (044) crystal planes of Fe$_3$O$_4$ (ICSD card number: 98-003-6314). These result confirmed our previous SEM observation that the magnetite particles had been successfully embedded in the biochar. Moreover, that the E-CMBC may capable of being separated from the aqueous solution by an external magnetic field after Pb(ii) adsorption.

The magnetic properties of E-CMBC was measured using vibrating sample magnetometry. The saturation magnetization value was 3.1 emu g^{-1} for E-CMBC, which was lower than that of bare magnetic particles (67 emu g^{-1}).[33] This may be due to the relatively low abundance of magnetic particles, as well as the

surface coating of chitosan and subsequent EDTA modification that caused lower magnetic strength. However, the E-CMBC remained separable and recoverable from the aqueous solution when a strong external magnetic field was applied. This property of E-CMBC is critical for its proposed recycling use in the removal of Pb(ii) from aqueous solutions.

3.2 Effect of adsorbent dosage

The effects of E-CMBC dosage on the adsorption capacity and removal efficiency of Pb(ii) were studied. As shown in Fig. 4a, the removal efficiency increased from 16.04% to 99.58% with increasing E-CMBC dosage from 0.2 to 2.0 g L^{-1}, while the adsorption capacity decreased from 160.4 mg g^{-1} to 99.63 mg g^{-1}. Consequently, the optimum adsorbent dosage was maintained at 1.0 g L^{-1} in the following experiments, which could guarantee excellent removal efficiency and adsorption capacity at the same time.

3.3 Effect of initial solution pH

It is well known that the initial solution pH is a significant factor that influences the protonation of the surface groups of the absorbent and the speciation of metal ions.[35] Therefore, it is necessary to optimize the pH to obtain the maximum adsorption efficiency. The effects of the initial solution pH on Pb(ii) adsorption by BC and E-CMBC are presented in Fig. 4b. To avoid
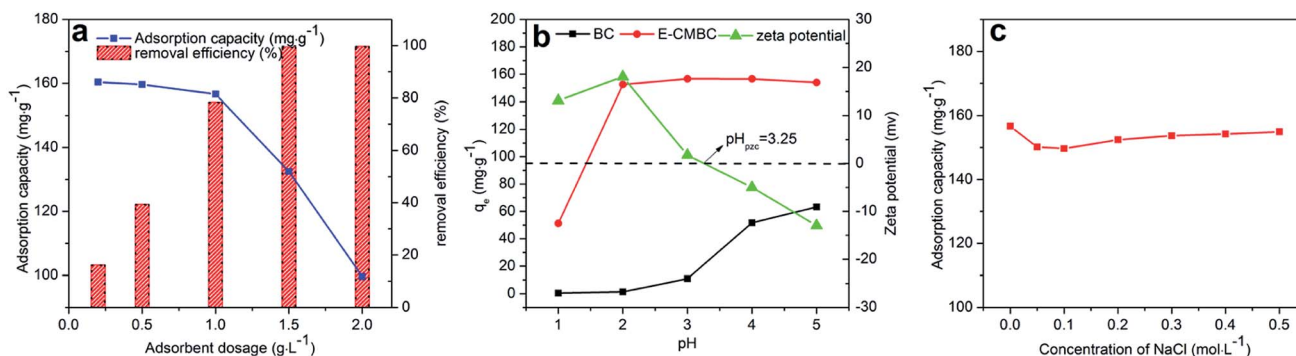

Fig. 4 (a) Effect of E-CMBC dosage on adsorption capacity and removal percentage of Pb(ii); (b) effect of initial solution pH and zeta potential on Pb(ii) adsorption for BC and E-CMBC; (c) effect of ionic strength on Pb(ii) adsorption for E-CMBC.

This journal is © The Royal Society of Chemistry 2020

Pb(II) precipitation, this study was conducted across different pH conditions ranging from 1.0 to 5.0.[41]

At pH 1.0, the adsorption of Pb(II) reached its minimum values of 0.5 mg g^{-1} and 51.2 mg g^{-1} for BC and E-CMBC, respectively. These results were obtained because of the stronger competitive adsorption of H$^+$ with Pb(II) at lower pH values. This was especially true for surface functional groups, such as the phenolic hydroxyl group and carboxyl group.[35] With increasing pH, functional group deprotonation provided more chances to co-ordinate with Pb(II), leading to a greater adsorption ability. For BC, the sorption capacity increased slowly across the initial portion of the tested pH range (1.0–3.0). Absorption increased sharply over pH 3.0, peaking at 5.0. The adsorption of Pb(II) reached its maximum value of 63.52 mg g^{-1}. The adsorption capacity of E-CMBC adsorbents sharply increased when the initial solution pH increased from 1.0 to 2.0.

Although the pH$_{PZC}$ value of E-CMBC is 3.25, the adsorption capacity of Pb(II) reached its maximum value of 156.68 mg g^{-1} at pH 3.0. When the pH was above 3.0, the adsorption capacity gradually plateaued, suggesting that electrostatic interactions do not play a key role in the process of Pb(II) adsorption. The adsorption capacity of Pb(II) for E-CMBC was larger than that for BC under the same condition. This result was likely due to the modification, which introduced more amino and carboxyl groups on the surface of the absorbent. In summary, the novel E-CMBC adsorbent was more effective at adsorbing Pb(II) than the untreated biochar, especially across a strongly acidic range.

3.4 Effect of ionic strength

The effect of ionic strength on Pb(II) adsorption by E-CMBC was evaluated. Fig. 4c illustrates the Pb(II) adsorption on E-CMBC in different concentrations of NaCl solution (0–0.5 mol L^{-1}). As presented in Fig. 4c, the effect of ionic strength on Pb(II) adsorption was negligible. Similar results were reported by Lv et al.[42] It was likely attributed to that the complexation between Pb(II) and E-CMBC was stronger than that between Na$^+$ and E-CMBC. The bonding constant of Pb(II) and EDTA is much larger than that of Na$^+$(Pb(II) log K = 18.04, Na$^+$ log K = 1.66), so Pb(II) is more likely to bind to E-CMBC.

3.5 Effect of contact time and adsorption kinetics

We next investigated the effect of contact time on Pb(II) adsorption by E-CMBC. To do so, the contact time was varied from 10 to 2880 min. As shown in Fig. 5a, the Pb(II) adsorption process had two distinct phases: a rapid initial phase and a much slower sorption phase. The rapid increase in the initial adsorption capacity for Pb(II) might be attributable to the high availability of adsorption sites. Accordingly, the reduction of available adsorption sites with time led to reduced adsorption rate.[35] It is worth noting that the adsorption capacity of Pb(II) reached 99.82 mg g^{-1} within only 10 min of contact time. After 360 min of contact time, the adsorption capacity of Pb(II) reached 154.5 mg g^{-1}. Due to the small increase of the adsorption capacity after 360 min of mixing, contact time of 1440 min was selected for all subsequent equilibrium tests.

The adsorption kinetic model is commonly used to estimate adsorption capacity and understand the underlying adsorption mechanism. The adsorption data for Pb(II) at different time intervals were simulated by pseudo-first-order, pseudo-second-order, and Avrami fractional-order models. The models are expressed as follows:

$$q_t = q_e(1 - e^{-k_1 t}) \tag{2}$$

$$q_t = \frac{k_2 q_e^2 t}{1 + k_2 q_e t} \tag{3}$$

$$q_t = q_e[1 - e^{-(k_3 t)^n}] \tag{4}$$

where q_e (mg g^{-1}) is the adsorption amounts of Pb(II) by E-CMBC at equilibrium, and q_t (mg g^{-1}) is the adsorption amounts of Pb(II) at time t (min). The parameters k_1 (min^{-1}), k_2 (g mg^{-1} min^{-1}), and k_3 (min^{-1}) are the pseudo-first-order, pseudo-second-order and Avrami fractional-order model adsorption rate constants, respectively.

The applicability of the model was assessed by using standard coefficient (R^2) and standard deviation (SD), i.e., the higher R^2 and lower SD uncovered a better fitness of the kinetic model. The calculated results are shown in Table 2. For the Avrami fractional-order model, the correlation coefficient value R^2
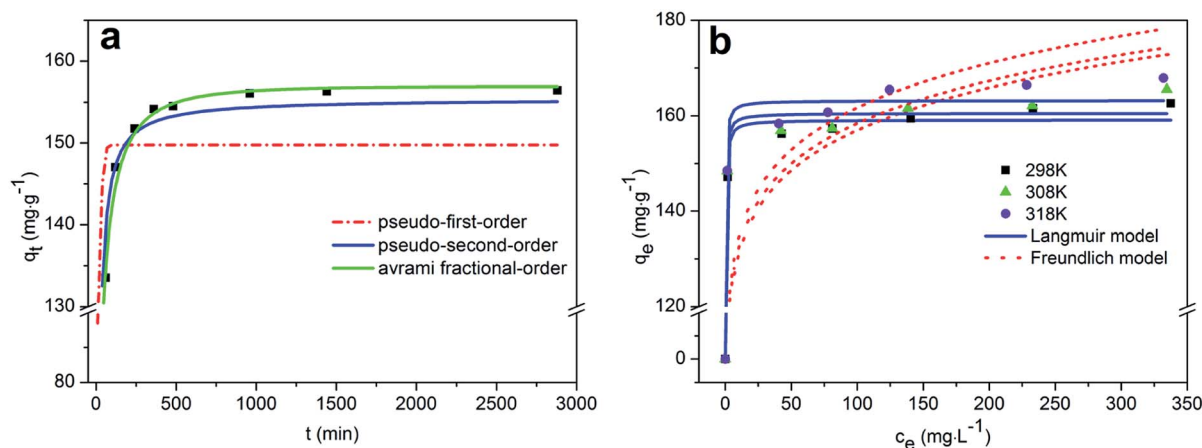

Fig. 5 (a) Adsorption kinetics of Pb(II) by E-CMBC and (b) adsorption isotherms of Pb(II) by E-CMBC.

Table 2 Kinetic model parameters for adsorption of Pb(II) by E-CMBC

Pseudo-first-order model		Pseudo-second-order model		Avrami fractional-order model	
q_e (mg g^{-1})	149.78	q_e (mg g^{-1})	155.43	q_e (mg g^{-1})	156.93
k_1 (min^{-1})	0.089	k_2 (min^{-1})	9.56×10^{-4}	k_3 (min^{-1})	0.096
R^2	0.68	R^2	0.95	R^2	0.99
SD	19.45	SD	6.76	SD	5.56

(0.99) was higher than that of the pseudo-first-order model (0.6806) and the pseudo-second-order model (0.95). The corresponding SD values were 19.45, 6.76 and 5.56, respectively. The calculated q_e had better agreement with the experimental values. Therefore, the Avrami fractional-order model is more suitable to describe the behavior of Pb(II) adsorption by E-CMBC, suggesting the adsorption of Pb(II) on E-CMBC is a multiple kinetics process.[43]

3.6 Adsorption isotherms

As is well known, adsorption isotherms are used to describe the equilibrium relationship between adsorbate and adsorbent.[44] To this end, Langmuir and Freundlich models are two widespread-used isotherm models. In this study, both of these models were adopted to simulate the experimental data and describe the adsorption characteristics between Pb(II) and E-CMBC. They are expressed as follows:

$$q_e = \frac{q_m K_L c_e}{1 + K_L c_e} \tag{5}$$

$$q_e = K_F c_e^{1/n} \tag{6}$$

$$R_L = \frac{1}{1 + K_L C_0} \tag{7}$$

where q_e (mg g^{-1}) is the adsorption capacity at equilibrium, q_m (mg g^{-1}) is the maximum adsorption capacity, c_0 (mg L^{-1}) is the initial concentration, and c_e (mg L^{-1}) is the concentration at equilibrium. K_L (L mg^{-1}) is the Langmuir constant related to the affinity of the binding sites, K_F is the Freundlich constant related to sorption capacity, n is the empirical parameter, and R_L is a dimensionless constant separation parameter.

The adsorption isotherms of Pb(II) by E-CMBC at 298 K, 308 K and 318 K are shown in Fig. 5b. As presented, the adsorption capacities increased with increasing c_e and approached the maximum adsorption capacities. The adsorption capacity also increased with increasing solution temperature. Here, the adsorption isotherms at different temperatures were further fitted with these two models, and the relevant parameters and normalized standard deviations are shown in Table 3. According to the coefficient correlation (R^2), the Langmuir model provided a better fit than the Freundlich model. This result suggested that the monolayer adsorption played a significant role in the Pb(II) adsorption process; moreover, that there was no interaction between the adsorbed molecules.[44] The constant K_L increased with increasing of temperature, indicating that the adsorption was an endothermic process. The parameter R_L could be used to describe the adsorption characteristics of the Langmuir model. As shown in Table 3, the calculated R_L values ($0 < R_L < 1$) indicated that the adsorption process was favorable at different temperatures.[45] These observations were consistent with those from previous studies of metal ion adsorption onto an adsorbent.[39,41,46,47] From Table 3, the maximum Pb(II) sorption capacity (163.19 mg g^{-1}) reported here was greater than that shown in many previous studies (Table 4), suggesting E-CMBC is a promising adsorbent for Pb(II) adsorption.

Table 3 Adsorption equilibrium constants obtained from Langmuir and Freundlich isotherms for the adsorption of Pb(II) by E-CMBC

Temperature (K)	Langmuir model				Freundlich model			
	q_m (mg g^{-1})	K_L (L mg^{-1})	R^2	SD	K_F (L mg^{-1})	n	R^2	SD
298	159.12	10.01	0.99	11.22	108.8	12.57	0.73	15.90
308	160.53	11.17	0.99	11.23	110.13	12.67	0.73	16.0
308	163.19	11.84	0.99	11.72	111.44	12.37	0.74	16.3

Table 4 Summary of various similar adsorbents for Pb(II) adsorption

Adsorbents	Conditions	Isotherm model	q_m (mg g^{-1})	Reference
Clanis bilineata larvae skin-derived biochars	pH 5.3, 25 °C	Langmuir	78	48
Chitosan	pH 6, 25 °C	Langmuir	13.6	49
Chitosan-modified biochar	pH 5, 45 °C	Langmuir	134	41
Chitosan/magnetite composite	pH 6, 25 °C	Langmuir	63.33	50
EDTA modified β-cyclodextrin/chitosan	pH 5, 45 °C	Langmuir	114.8	44
EDTA-modified chitosan–silica hybrid	pH 3, 22 °C	Bi-Langmuir and Sips	89.01	51
EDTA-modified chitosan/magnetic biochar	pH 3, 45 °C	Langmuir	163.19	This study

Table 5 Thermodynamic parameters for the adsorption of Pb(II) by E-CMBC

T (K)	ln K_d	ΔG (kJ mol^{-1})	ΔH (kJ mol^{-1})	ΔS (J mol^{-1} K^{-1})
298	1.30	−3.12	3.95	23.74
308	1.32	−3.37		
318	1.36	−3.60		

3.7 Adsorption thermodynamics

Thermodynamic analysis was used to describe the relationship between adsorption and temperature, with the intent of obtaining information to further understand the adsorption process of E-CMBC for Pb(II). The thermodynamic parameters of free energy change (ΔG), enthalpy change (ΔH), and entropy change (ΔS) were calculated from the following equations:

$$K_d = \frac{q_e}{c_e} \tag{8}$$

$$\ln K_d = \frac{\Delta S}{R} - \frac{\Delta H}{RT} \tag{9}$$

$$\Delta G = \Delta H - T \times \Delta S \tag{10}$$

where q_e (mg g^{-1}) is the adsorption capacity at equilibrium, c_e (mg L^{-1}) is the concentration at equilibrium, K_d is the adsorption equilibrium constant, R (8.314 J mol^{-1} K^{-1}) is the gas constant, and T (K) is the adsorption temperature.

Thermodynamic experiments were conducted at 298 K, 308 K, and 318 K and, results are shown in Table 5.

As shown in Table 5, ΔG negative values were −3.12 kJ mol^{-1}, −3.37 kJ mol^{-1}, and −3.60 kJ mol^{-1} at 298 K, 308 K, and 318 K, respectively. As temperature increased, ΔG values became increasingly more negative, which indicated that the adsorption was spontaneous. Moreover, this spontaneity was easier with increased temperature.[34] The positive value of ΔH was 3.948 kJ mol^{-1}, implying an endothermic sorption.[39] Furthermore, the positive value of ΔS was 23.74 J mol^{-1} K^{-1}, implying increased randomness at the solid–solution interface

Fig. 6 Proposed adsorption mechanism of Pb(II) by E-CMBC.

during the adsorption process.[44] Collectively, these results indicated that the sorption of Pb(II) by E-CMBC was a spontaneous and endothermic process.

3.8 Desorption and regeneration studies

The reusability of an adsorbent is an important, practical feature and we next tested the adsorption–desorption cycle of E-CMBC for Pb(II). After three adsorption–desorption cycles, the E-CMBC removal efficiency of Pb(II) reached 97.26%, with 78.60% weight recovered. Therefore, it seemed that the EDTA modification stabilized the adsorbent and allowed it to better resist the acidic environment. Taken together, this indicated that E-CMBC has an excellent reusability.
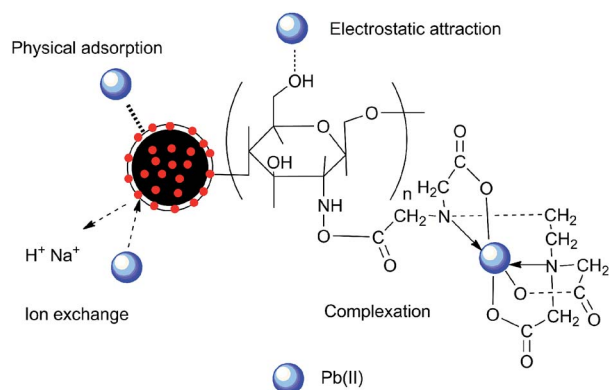
3.9 Adsorption mechanisms

In this study, a possible mechanism for these results has been proposed (Fig. 6), which is summarized as follows: (1) complex of Pb(II) and EDTA groups; (2) electrostatic attraction between Pb(II) with –NH$_2$ groups and –OH groups; (3) ion exchange between Na$^+$ and Pb(II); (4) physical adsorption of Pb(II) by E-CMBC materials.

Table 1 shows the adsorption capacity of BC, MBC, CMBC and E-CMBC for Pb(II). After each step of biochar modification, the adsorption capacity of Pb(II) increased. This was especially true after EDTA modification, where the adsorption capacity increased sharply. These results may be due to the appearance of amides and carboxyl groups on the surface of E-CMBC.

The FTIR spectra of E-CMBC before and after Pb(II) adsorption were also used to study the adsorption mechanism (Fig. 3b). When compared with the FTIR spectrum of E-CMBC, the overlapping peaks of the –OH and –NH$_2$ group vibrations shifted from 3416 to 3230 cm^{-1} after Pb(II) adsorption. These results indicated that these groups might interact with Pb(II).[44] The stretching vibration peak of C=O (–NH–C=O and –COOH) shifted from 1653 cm^{-1}, and 1407 cm^{-1} to 1624 cm^{-1}, and 1375 cm^{-1} and the intensity decreased relative to other peaks. This was due to the complexation of amine and carboxyl functional groups with Pb(II).[52] These results confirmed the inference that both amides and carboxyl groups played a key role in the process of Pb(II) adsorption.

The XPS analyses were used to confirm the adsorption mechanism of E-CMBC for Pb(II). As shown in Fig. 3a, the typical new peaks of Pb 4p$_3$, Pb 4d$_3$, Pb 4d$_5$, Pb 4f$_{7/2}$, and Pb 4f$_{5/2}$ appeared at 652.08 eV, 401.08 eV, 415.08 eV, 437.08 eV, 138.93 eV, and 143.78 eV, respectively. These results indicated the presence of Pb(II) in the E-CMBC after adsorption. Notably, the binding energy of Pb 4f$_{7/2}$ became slightly lower than that of Pb(NO$_3$)$_2$ (139.1–139.5 eV), confirming the formation of a complex between Pb(II) and the EDTA group of E-CMBC during the adsorption process.[42] From the full-range XPS of E-CMBC before and after adsorption, the typical peaks of Na$_{1s}$ around 1072.08 eV disappeared after sorption. This was mainly due to the exchange of Na$^+$ on the surface of E-CMBC with Pb(II).

In addition to the three mechanisms mentioned above, physical adsorption was also a common adsorption mechanism of E-CMBC, as it is a porous material.[42] Moreover, the collective

results of the adsorption kinetics and isotherm experiments showed that chemisorption on the monolayer surface played a dominant role. According to the analysis above, complexation played a major role in the removal of Pb(II) by E-CMBC, while the other three mechanisms played relatively weaker roles.

4. Conclusions

In this study, a novel magnetic and recyclable biochar adsorbent was successfully synthesized by modification with both chitosan and EDTA. This novel biochar was made for the removal of Pb(II) from aqueous solutions. The E-MCBC absorbent exhibited excellent adsorption performance for Pb(II) even under strongly acidic conditions. Both the Avrami fractional-order model and Langmuir isotherm model had better fit for the adsorption data, while the Langmuir maximum adsorption capacity was 159.12 mg g^{-1}, which was 14 times higher than that of BC. Even at pH 2.0, the adsorption capacity could reached 152.5 mg g^{-1}, suggesting that the novel magnetic biochar adsorbent was not affected by strongly acidic conditions. To the best of our knowledge, this is the first report of such a property. A subsequent mechanistic analysis suggested that the complexation of –NH–C═O and –COOH groups on the surface of E-CMBC with Pb(II) was the governing mechanism for the dramatic improvement in its adsorption capacity. The magnetic property of E-CMBC enabled the easy separation of consumed adsorbent from wastewater. In general, as a novel, recyclable and highly efficient adsorbent, E-CMBC has great potential for use in the treatment of Pb(II) polluted wastewater. Future research will focus on the E-CMBC on other toxic heavy metal and metal loids along with mixed contaminants in pilot-scaled tests.

Conflicts of interest

There are no conflicts to declare.

Acknowledgements

References

1 Y. Zhang, D. Hou, O. David, Z. Shen, P. Shi, Y. S. Ok, D. C. W. Tsang, Y. Wen and M. Luo, *Crit. Rev. Environ. Sci. Technol.*, 2019, **49**, 1386–1423.

2 X. Ren, S. Yang, D. Shao and X. Tan, *Sep. Sci. Technol.*, 2013, **48**, 1211–1219.

3 D. Mohan, C. U. Pittman Jr, M. Bricka, F. Smith, B. Yancey, J. Mohammad, P. H. Steele, M. F. Alexandre-Franco, V. Gómez-Serrano and H. Gong, *J. Colloid Interface Sci.*, 2007, **310**, 57–73.

4 M. Kobya, E. Demirbas, E. Senturk and M. Ince, *Bioresour. Technol.*, 2005, **96**, 1518–1521.

5 X. Yang, Y. Wan, Y. Zheng, F. He, Z. Yue, J. Huang, H. Wang, Y. S. Ok, Y. Jiang and B. Gao, *Chem. Eng. J.*, 2019, **366**, 608–621.

6 G. Zhao, J. Li, X. Ren, C. Chen and X. Wang, *Environ. Sci. Technol.*, 2011, **45**, 10454–10462.

7 R. Xiao, S. Wang, R. Li, J. J. Wang and Z. Zhang, *Ecotoxicol. Environ. Saf.*, 2017, **141**, 17–24.

8 D. Sud, G. Mahajan and M. P. Kaur, *Bioresour. Technol.*, 2008, **99**, 6017–6027.

9 H. Chen, Y. Teng, S. Lu, Y. Wang and J. Wang, *Sci. Total Environ.*, 2015, **512–513**, 143–153.

10 M. K. Uddin, *Chem. Eng. J.*, 2017, **308**, 438–462.

11 Q. Wu, H. Zhou, N. F. Y. Tam, Y. Tian, Y. Tan, S. Zhou, Q. Li, Y. Chen and J. Y. S. Leung, *Mar. Pollut. Bull.*, 2016, **104**, 153–161.

12 D. Shao, C. Chen and X. Wang, *Chem. Eng. J.*, 2012, **185–186**, 144–150.

13 L. Yan, L. Kong, Z. Qu, L. Li and G. Shen, *ACS Sustainable Chem. Eng.*, 2015, **3**, 125–132.

14 R. Hu, X. Wang, S. Dai, D. Shao, T. Hayat and A. Alsaedi, *Chem. Eng. J.*, 2015, **260**, 469–477.

15 Y. Zou, X. Wang, A. Khan, P. Wang, Y. Liu, A. Alsaedi, T. Hayat and X. Wang, *Environ. Sci. Technol.*, 2016, **50**, 7290–7304.

16 M. Arshadi, M. Soleymanzadeh, J. W. L. Salvacion and F. Salimi Vahid, *J. Colloid Interface Sci.*, 2014, **426**, 241–251.

17 A. Bashir, L. A. Malik, S. Ahad, T. Manzoor, M. A. Bhat, G. N. Dar and A. H. Pandith, *Environ. Chem. Lett.*, 2019, **17**, 729–754.

18 G. Macchi, D. Marani, M. Pagano and G. Bagnuolo, *Water Res.*, 1996, **30**, 3032–3036.

19 J. P. Bezzina, L. R. Ruder, R. Dawson and M. D. Ogden, *Water Res.*, 2019, **158**, 257–267.

20 C. A. Basha, M. Somasundaram, T. Kannadasan and C. W. Lee, *Chem. Eng. J.*, 2011, **171**, 563–571.

21 S. Zhang, Q. Shi, C. Christodoulatos, G. Korfiatis and X. Meng, *Chem. Eng. J.*, 2019, **370**, 1262–1273.

22 J. Ma, M. Xia, S. Zhu and F. Wang, *J. Hazard. Mater.*, 2020, **400**, 123143.

23 L. Dupont and E. Guillon, *Environ. Sci. Technol.*, 2003, **37**, 4235–4241.

24 Y. Zhou, X. Liu, T. Lin, F. Zhang, G. Zeng, X. Peng, L. Luo, Y. Deng, Y. Pang and J. Zhang, *J. Hazard. Mater.*, 2017, **333**, 80–87.

25 J. Sun, L. Wu and Y. Li, *J. Taiwan Inst. Chem. Eng.*, 2017, **78**, 219–229.

26 A. I. A. Sherlala, A. A. A. Raman, M. M. Bello and A. Asghar, *Chemospher*, 2018, **193**, 1004–1017.

27 N. Chanthapon, S. Sarkar, P. Kidkhunthod and S. Padungthon, *Chem. Eng. J.*, 2018, **331**, 545–555.

28 R. Karthik and S. Meenaksh, *Chem. Eng. J.*, 2015, **263**, 168–177.

29 E. B. Son, K. M. Poo, H. O. Mohamed, Y. J. Choi, W. C. Cho and K. J. Chae, *Bioresour. Technol.*, 2018, **259**, 381–387.

30 K. R. Thines, E. C. Abdullah, N. M Mubarak and M. Ruthiraan, *Renewable Sustainable Energy Rev.*, 2017, **67**, 257–276.

31 J. Qu, M. S. Akindolie, Y. Feng, Z. Jiang, G. Zhang, Q. Jiang, F. Deng, B. Cao and Y. Zhang, *Chem. Eng. J.*, 2020, **394**, 124915.

32 E. B. Son, K. M. Poo, J. S. Chang and K. J. Chae, *Sci. Total Environ.*, 2018, **615**, 161–168.

33 S. Liu, B. Huang, L. Chai, Y. Liu, G. Zeng, X. Wang, W. Zeng, M. Shang, J. Deng and Z. Zhou, *RSC Adv.*, 2017, **7**, 10891–10899.

34 J. Deng, Y. Liu, S. Liu, G. Zeng, X. Tan, B. Huang, X. Tang, S. Wang, Q. Hua and Z. Yan, *J. Colloid Interface Sci.*, 2017, **506**, 355–364.

35 F. Xiao, J. Cheng, W. Cao, C. Yang, J. Chen and Z. Luo, *J. Colloid Interface Sci.*, 2019, **540**, 579–584.

36 J. Wang and S. Zhuang, *Crit. Rev. Environ. Sci. Technol.*, 2017, **47**, 2331–2386.

37 E. Repo, J. K. Warchoł, A. Bhatnagar, A. Mudhoo and M. Sillanpää, *Water Res.*, 2013, **47**, 4812–4832.

38 M. Zhang, B. Gao, S. Varnoosfaderani, A. Hebard, Y. Yao and M. Inyang, *Bioresour. Technol.*, 2013, **130**, 457–462.

39 R. Li, W. Liang, H. Huang, S. Jiang, D. Guo, M. Li, Z. Zhang, A. Ali and J. J. Wang, *J. Appl. Polym. Sci.*, 2018, **135**, 46239.

40 A. Ayati, B. Tanhaei and M. Sillanpää, *J. Appl. Polym. Sci.*, 2017, **134**, 44360.

41 N. B. Dewage, R. E. Fowler, C. U. Pittman Jr, D. Mohan and T. Mlsna, *RSC Adv.*, 2018, **8**, 25368–25377.

42 D. Lv, Y. Liu, J. Zhou, K. Yang, Z. Lou, S. A. Baig and X. Xu, *Appl. Surf. Sci.*, 2018, **428**, 648–658.

43 J. Qu, Y. Liu, L. Cheng, Z. Jiang, G. Zhang, F. Deng, L. Wang, W. Han and Y. Zhang, *J. Hazard. Mater.*, 2021, **403**, 123607.

44 D. Wu, L. Hu, Y. Wang, Q. Wei, L. Yan, T. Yan, Y. Li and B. Du, *J. Colloid Interface Sci.*, 2018, **523**, 56–64.

45 C. Wang and H. Wang, *Chemosphere*, 2018, **192**, 1–4.

46 J. Aguado, J. M. Arsuaga, A. Arencibia, M. Lindo and V. Gascón, *J. Hazard. Mater.*, 2009, **163**, 213–221.

47 D. Mohan, H. Kumar, A. Sarswat, M. Alexandre-Franco and C. U. Pittman Jr, *Chem. Eng. J.*, 2014, **236**, 513–528.

48 Y. Yan, L. Zhang, Y. Wang, X. Wang, S. Wang, Q. Li, X. Liu, Y. Xu, J. Yang and N. Bolan, *Sci. Total Environ.*, 2020, **704**, 135251.

49 C. Huang, Y. Chung and M. Liou, *J. Hazard. Mater.*, 2009, **45**, 265–277.

50 H. V. Tran, L. D. Tran and T. N. Nguyen, *Mater. Sci. Eng., C*, 2010, **30**, 304–310.

51 E. Repo, J. K. Warchoł, A. Bhatnagar and M. Sillanpää, *J. Colloid Interface Sci.*, 2011, **358**, 261–267.

52 Y. Liu, R. Fu, Y. Sun, X. Zhou, S. Baig and X. Xu, *Appl. Surf. Sci.*, 2016, **369**, 267–276.